Nie *et al. Earth, Planets and Space* (2018) 70:55
https://doi.org/10.1186/s40623-018-0826-4

Earth, Planets and Space

FULL PAPER

Open Access

Fault model of the 2017 Jiuzhaigou Mw 6.5 earthquake estimated from coseismic deformation observed using Global Positioning System and Interferometric Synthetic Aperture Radar data

Zhaosheng Nie, Di-Jin Wang*, Zhige Jia, Pengfei Yu and Liangfa Li

Abstract

On August 8, 2017, the Jiuzhaigou Mw 6.5 earthquake occurred in Sichuan province, southwestern China, along the eastern margin of the Tibetan Plateau. The epicenter is surrounded by the Minjiang, Huya, and Tazang Faults. As the seismic activity and tectonics are very complicated, there is controversy regarding the accurate location of the epicenter and the seismic fault of the Jiuzhaigou earthquake. To investigate these aspects, first, the coseismic deformation field was derived from Global Positioning System (GPS) and Interferometric Synthetic Aperture Radar (InSAR) measurements. Second, the fault geometry, coseismic slip model, and Coulomb stress changes around the seismic region were calculated using a homogeneous elastic half-space model. The coseismic deformation field derived from InSAR measurements shows that this event was mainly dominated by a left-lateral strike-slip fault. The maximal and minimal displacements were approximately 0.15 m and −0.21 m, respectively, along line-of-sight observation. The whole deformation field follows a northwest-trending direction and is mainly concentrated west of the fault. The coseismic slip is 28 km along the strike and 18 km along the dip. It is dominated by a left-lateral strike-slip fault. The average and maximal fault slip is 0.18 and 0.85 m, respectively. The rupture did not fully reach the ground surface. The focal mechanism derived from GPS and InSAR data is consistent with the kinematics and geometry of the Huya Fault. Therefore, we conclude that the northern section or the Shuzheng segment of the Huya Fault is the seismogenic fault. The maximal fault slip is located at 33.25°N and 103.82°E at a depth of ~ 11 km, and the release moment is approximately 6.635×10^{18} Nm, corresponding to a magnitude of Mw 6.49, which is consistent with results reported by the US Geological Survey, Global Centroid Moment Tensor, and other researchers. The coseismic Coulomb stress changes enhanced the stress on the northwest and southeast edges of the northern extension of the Huya Fault. Seismic risks cannot be ignored in the future although aftershocks are fewer in number in these regions.

Keywords: 2017 Jiuzhaigou earthquake, Coseismic slip model, GPS, InSAR, Coulomb stress change

*Correspondence: wangdijin@126.com
Key Laboratory of Earthquake Geodesy, Institute of Seismology, Chinese Earthquake Administration, Wuhan, China

Introduction

A strong earthquake occurred on August 8, 2017, in Jiuzhaigou county of the Aba region in northern Sichuan province, China, resulting in 25 deaths, 525 injuries, and extensive damage to buildings. The China Earthquake Networks Center (CENC) determined the magnitude was Ms 7.0 and the epicenter was at 33.20°N and 103.88°E, with a focal depth of 20 km (Fig. 1a). The US Geological Survey (USGS) and Global Centroid Moment Tensor (GCMT) Catalog also released the focal mechanism solutions of the earthquake, indicating the magnitude was Mw 6.5 and it was a strike-slip event.

The Jiuzhaigou earthquake occurred in the northeastern part of the Tibetan Plateau. It occurred on the eastern edge of the Bayan Har block, a region with complex and varied geological structure (Liu et al. 2006; Wang et al. 2007). The frequent occurrence of strong earthquakes is direct evidence of the tectonic activities of the Bayan Har block, which is a secondary block of the Tibetan Plateau in which earthquake activity has been very strong during recent years (Deng et al. 2014). The eastern Bayan Har block and its vicinity is the leading edge of the Tibetan Plateau. Meanwhile, the Jiuzhaigou earthquake occurred in the middle of China's north–south seismic belt. The nucleation and occurrence of strong earthquakes depend strongly on tectonic activities over a long timescale, in particular, the crustal deformation of active blocks. The Jiuzhaigou earthquake occurred in the vicinity of the eastern edge of the Bayan Har block, indicating that the block is still active. It is noted that a number of destructive earthquakes have occurred on the boundary of the Bayan Har block since the Mw 7.6 Manyi earthquake in 1997 (Liu et al. 2006). Because the stress transfer caused by strong earthquakes may trigger new earthquakes (Stein 2003), it is important to determine the position and geometry of the seismogenic fault and the coseismic slip model. Based on the seismic stress trigger theory, the study of static Coulomb stress changes resulting from a strong earthquake is very helpful to more fully understand seismic activities that serve to assess the occurrence risk of high-magnitude earthquakes in the future (Xiong et al. 2015; Shan et al. 2012). Because of different opinions on the accurate location of the epicenter and the seismogenic fault of the Jiuzhaigou earthquake, in this study we conducted a joint inversion from coseismic Global Positioning System (GPS) and Interferometric Synthetic Aperture Radar (InSAR) measurements to identify the focal mechanism as well as future impacts on surrounding faults.

Tectonic and crustal deformation settings

The epicenter of the Jiuzhaigou Mw 6.5 earthquake is at the intersection of three tectonic faults: the Tazang, Minjiang, and Huya Faults (Fig. 1a). The catalog of historical earthquakes shows that this area has been subjected to many moderately strong earthquakes. The strongest earthquake was the M8 Wudu earthquake that occurred in 1879 75 km east of the Jiuzhaigou earthquake. The most recent strong earthquake was the Songpan earthquake sequence that occurred on the Huya Fault in 1976 (Tang and Lu 1981) 60–80 km southeast of the Jiuzhaigou earthquake (Fig. 1a). The epicenter of the Jiuzhaigou earthquake as determined by a number of institutes is far from the Minjiang Fault as compared to the other two faults; thus, the Minjiang Fault can be excluded as the possible seismogenic fault. Situated on the eastern edge of the Minshan uplift zone, the Huya Fault is northwest of the Longmenshan Fault, generally trending to the N-NW. It may be divided into northern and southern sections separated by Xiaohe. The strike of the northern section changes from SE-E to SE with a dip of ~ 80°. The strike of the southern section changes from NS to SE and dips westward. The dip angle changes from 70° to 30° from north to south (Tang and Lu 1981). Four moderately strong earthquakes have occurred recorded Huya Fault historical seismicity. The largest was two M7.2 mainshocks of the Songpan earthquake sequence in 1976. The M6.5 Songpan-Huanglong earthquake in 1973 was the nearest event, occurring 30 km south of the epicenter of the Jiuzhaigou earthquake (Fig. 1a). The focal mechanism solutions of the Songpan earthquakes of 1976 indicated that this event on the Huya Fault was a left-lateral slip event (Jones et al. 1984). Zhou et al. (2007) investigated the geological and geomorphological characteristics of the area since the late Quaternary and concluded that the average left-slip rate and vertical slip rate of the Huya Fault are 1.4 and 0.3 mm/a, respectively.

The Tazang Fault is along the eastern section of the eastern Kunlun Fault. It is a left-lateral strike-slip fault, generally trending to the NW with the shape of a reversed S. The Tazang Fault is divided into three sections from west to east: the Luocha, Dongbeicun, and Majiamo sections. The strikes of the three sections are 113°, 142°, and 130°, respectively. Fault deformation patterns during the late Quaternary exhibited were multi-segment and multi-phase. During the Holocene, the Luocha segment was dominated by left-lateral strike-slip shear with velocities ranging from 2.43 to 2.89 mm/a (Hu et al. 2017). The nearest segment to the Jiuzhaigou earthquake is the Majiamo section, which trends to the NW-W, starting from Zhangzha and extending toward the southeast with a dip angle of from 40° to 65°. The total length is ~ 60 km (Fu et al. 2017; Hu et al. 2017). The slip rate of the Tazang Fault decreases from 12.5 mm/a in its

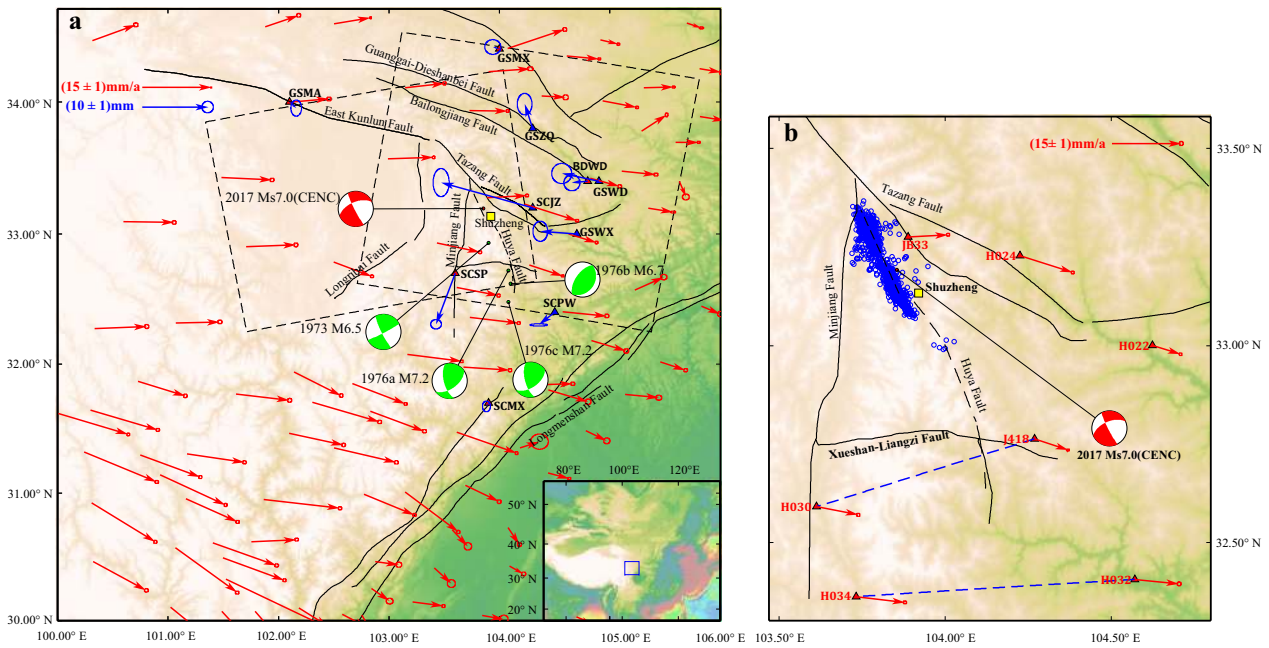

Fig. 1 **a** Topography, faults, GPS velocity field with 95% confidence ellipses relative to the Eurasian Plate, coseismic horizontal GPS deformation and Sentinel-1A SAR image range in the epicenter and the surrounding area of the Jiuzhaigou earthquake. The black curved lines represent faults. The black dashed quadrilaterals represent the area covered by the descending and ascending Sentinel-1A images. The red triangles represent continuous GPS stations of the Crustal Movement Observation Network of China and the blue triangles the Beidou Ground Based Augmentation System stations. The red arrows represent the horizontal velocity field before the earthquake, and the blue arrows represent the coseismic deformation of the horizontal component. **b** Aftershock distribution, tectonic setting, and GPS velocity with 95% confidence ellipses relative to the Eurasian Plate

mid-section to ~1 mm/a at the end of the eastern Kunlun Fault (Kirby et al. 2007). The thrust movement decreases from 1.5 mm/a in the west to ~0.2–0.3 mm/a in the east (Ren et al. 2013). Because of the complex geological structure near the epicenter of the Jiuzhaigou earthquake, the southern end of the Tazang Fault is relatively close to the northern section of the Huya Fault, and thus, it is difficult to identify the seismogenic fault of Jiuzhaigou event. According to the distribution of aftershocks (Fig. 1b), the seismogenic fault of this earthquake may be a blind fault extending to the northwest of the Huya Fault or the Tazang Fault northeast of the epicenter.

Present-day crustal deformation monitoring of the seismic region relies mainly on GPS observation. Wang et al. (2008) made use of GPS data of the Minshan block from prior to the Wenchuan earthquake over a span of 10 years to derive the velocity of this region. The crustal shortening rate is approximately 2 mm/a for the Huya Fault. Using horizontal GPS velocities between 2013 and 2015 from the latest data of the Crustal Movement Observation Network of China (CMONOC) (Fig. 1a), we inverted the slip rates across the Huya Fault using a profile projection method. Two pairs of GPS sites spanning the south and north sections of the Huya Fault were chosen to obtain the deformation patterns after the Wenchuan earthquake (Table 1). The deformation of the entire fault exhibited a pattern of left-lateral and thrust motion. This is generally in agreement with the geological results. However, the rate of slip showed a slight discrepancy compared to the geological results. The motion rates in the northern section were faster than those of the southern section; thus, discrepancies in the deformation patterns existed as well (Table 1).

Geodetic observations, processing, and analysis

The GPS data used in this study originated from the CMONOC and the continuous stations of the Beidou Ground Based Augmentation System (BGBAS) within 150 km from the epicenter. The nearest stations to the epicenter are the SCJZ (BGBAS) and SCSP (CMONOC) stations 40 and 65 km away, respectively (Fig. 1a). Because of the lack of available processing software for the Beidou measurements, we only used the GPS data acquired at 30-s samples of 10 days before the earthquake and 4 days after the earthquake. Using GAMIT/GLBOK software and the final precise ephemeris, we calculated the horizontal coseismic displacement of the earthquake (Fig. 1a). Results show that the earthquake resulted in significant horizontal coseismic deformation at both SCJZ and SCSP. The displacement was 14.28 and

Table 1 Kinematic characteristics of the southern and northern sections of the Huya Fault derived from GPS velocities between 2013 and 2015

Profiles	GPS pairs	Slip rate (mm/a) in the trending direction	Slip rate (mm/a) perpendicular to the fault strike	Kinematics of the fault
Northern section	J418 and H030	0.54	1.28	Left-lateral with thrust
Southern section	H032 and H034	−0.02	0.46	Left-lateral

Table 2 InSAR information for Sentinel-1A images

No.	Mode	Acquisition time		Temporal baseline (d)	Perpendicular baseline (m)
		Master	Slave		
1	Ascending	2017-07-30	2017-08-11	12	35
2	Descending	2017-08-06	2017-08-12	6	−92

8.20 mm, respectively. These two stations are situated on either side of the Huya Fault. The coseismic offset displaced to the NW and SW, respectively, indicating that the coseismic deformation consisted of a left-lateral slip component.

The European Space Agency (ESA) quickly released interferometric wide (IW) mode observations of the Jiuzhaigou region imaged by the Sentinel-1A (C-band) satellite along ascending and descending orbits following the Jiuzhaigou earthquake (Fig. 1a and Table 2). The Scientific Computing Environment (ISCE) InSAR software jointly developed by the Jet Propulsion Laboratory (JPL) and Stanford University was used to process the Sentinel-1A data. Precise orbits released by the ESA and 30-m Shuttle Radar Topography Mission (SRTM) digital elevation models from National Aeronautics and Space Administration (NASA) were used to remove the topographic signature from the InSAR phases (Farr and Kobrick 2000). Interferograms were derived using a multi-look factor of 10 in range and 2 in azimuth. In addition, a weighted power spectrum method was used to filter fringes to generate the wrapped interferograms (Goldstein and Werner 1998). A minimum cost flow method was performed to unwrap the filtered phase. Finally, the unwrapped interferograms were geocoded to a geographic coordinate system and then converted to line-of-sight (LOS) displacements (Fig. 2). A root-mean-square (RMS) error of the interferogram was estimated to assess the precision of InSAR. We used the one-dimensional (1-D) covariance function to describe the RMS characteristics (Parsons et al. 2006). The RMS for InSAR is approximately 1.5 mm, indicating the interferogram is slightly affected by atmospheric disturbance.

The interferograms present good coherence and the fringes are relatively continuous because the spatiotemporal baselines used are short (Fig. 2 and Table 2). The coseismic deformation field of LOS obtained from the ascending track data (Fig. 2a, c) presents a shape of a long flat oblate with the long axis trending to the NW with a maximal uplift and subsidence of 0.07 and 0.21 m, respectively. The deformation on both sides of the fault is asymmetric. However, the displacements are mainly concentrated on the west side of the fault, indicating that the fault is dipping to the west. The overall deformation pattern has a subsidence style with slight uplift in the south. The maximal deformation region of the coseismic field obtained from the descending track data is fundamentally consistent with that of the subsidence region obtained from the ascending track data. The deformation is mainly concentrated on the west side of the fault, and the maximal uplift and subsidence are 0.16 and 0.08 m, respectively. The dislocation characteristics obtained from the ascending and descending data have some discrepancies. This is mainly related to the imaging geometry of the satellite and the direction of the surface deformation.

Wang et al. (2014) first used a quadtree algorithm to downsample the InSAR coseismic deformation field along with the corresponding incidence and azimuth of each pixel to improve the inverse calculation efficiency (Lohman and Sinmons 2005). During the quadtree downsampling process in this study, the deformation gradient threshold was set to 0.3 for the near-field region to obtain a higher density of sampling points to employ a tight constraint on the inversion computation. For the far field, the deformation gradient threshold was set to 0.5 to obtain a set of relatively sparse points. Although the final downsampled points totaled 2202, the spatial characteristics of the coseismic deformation can be retained to a maximum extent.

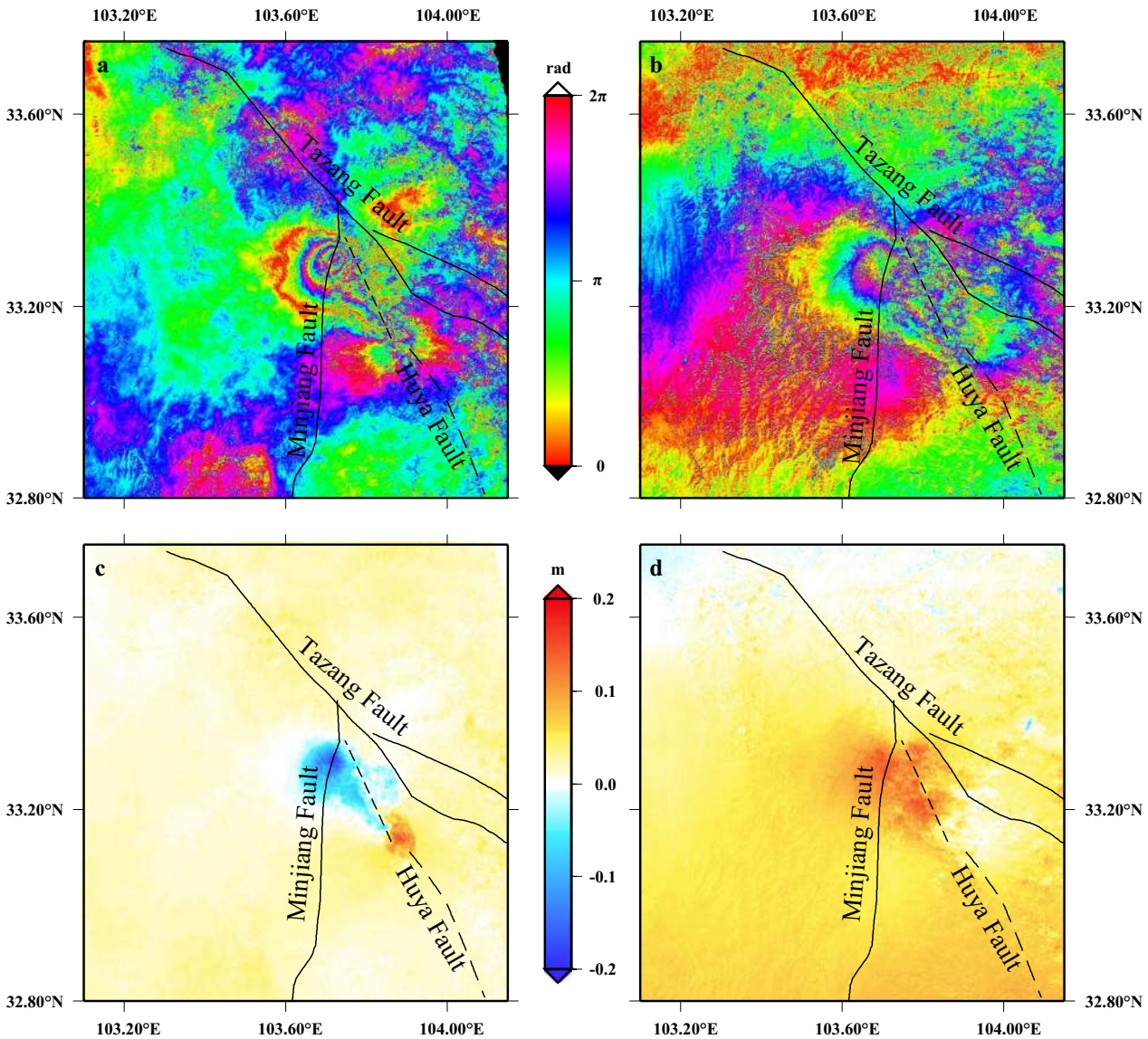

Fig. 2 Coseismic deformation of the Jiuzhaigou earthquake from InSAR. **a**, **c** Present the interferogram and LOS displacements along the ascending orbit. **b**, **d** Present the interferogram and LOS displacements along the descending orbit

Inversion for fault geometry and coseismic slip model

The geometric parameters of the seismogenic fault were initially determined on the basis of precise relocation of aftershocks within 1 month as well as the coseismic deformation patterns observed by InSAR. The focal mechanism solutions provided by the USGS and GCMT show that the strike of the seismogenic fault is 153° and 150°, respectively, which is consistent with the long axis direction of the aftershock relocations. Meanwhile, the InSAR ascending interferogram indicates the NW fringe is steeper in a NE direction and the southwest gradient is gentler, indicating that the surface projection trace of the fault should trend to the SE. Regarding the dip angle, we set it to a range of from 60° to 90° based on the geological results and the focal mechanism solutions provided by many institutions (Shan et al. 2017b; Yi et al. 2017). The range of aftershocks is generally larger than that of the coseismic rupture (Wells and Coppersmith 1994). The fault length and width were set to 40 km and 30 km, respectively, by combining the focal mechanism solutions and many trial computations. The fault plane was divided into 20×15 sub-faults of 2 km $\times$ 2 km along the strike and dip direction.

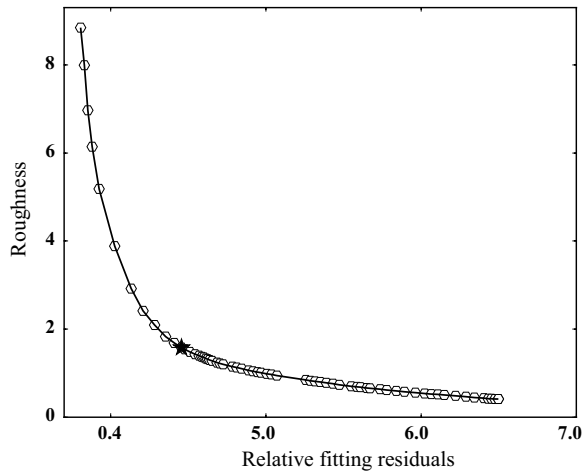

Fig. 3 Trade-off curve of relative fitting residuals and roughness. The pentagram is the position of the smooth factor used

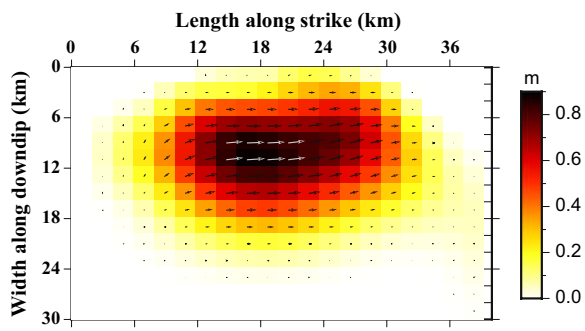

Fig. 4 Coseismic slip model of the Jiuzhaigou earthquake

Using the mean value of the observation and the number of sampling points, we normalized various types of observational data to determine the relative weight ratio of GPS and InSAR data in the joint inversion. Considering that the relative position of GPS is precise, we set its relative weight to 1 and set the weight ratio interval of InSAR to (0, 1). The weighted ratio of the minimum fitting GPS residuals was chosen as the optimal relative weight ratio in this interval. A factor of 1:0.2 was chosen as the weight ratio of GPS and InSAR inversion after many calculations. The smoothing factor is generally determined by a trade-off curve of roughness and fitting residuals. We chose 0.08 as the best smoothing factor at the inflection point of the trade-off curve (Fig. 3). Finally, a fault slip model was obtained based on a homogeneous elastic half-space model (Okada 1985) (Fig. 4). Results demonstrated that the coseismic slip was mainly dominated by strike slip. The coseismic slip was mainly distributed for 28 km along the strike and 18 km along the dip. The average and maximal slip was 0.18 and 0.85 m, respectively. The maximal fault slip occurred at 33.25°N, 103.82°E at a depth of ~11 km. The dip and rake angles were 81° and −11°, respectively. The release moment was 6.635×10^{18} Nm, corresponding to a magnitude of Mw 6.49, which is consistent with the focal mechanism solutions obtained by the USGS and GCMT as well as others (Shan et al. 2017b; Wang et al. 2018; Yi et al. 2017).

According to the distribution of the residuals between the observed and simulated coseismic deformation using GPS (Fig. 5), the simulated results of GPS stations close to the epicenter were better and the direction of the simulated value was consistent with the observed value and their differences were less than 2 mm. The residuals

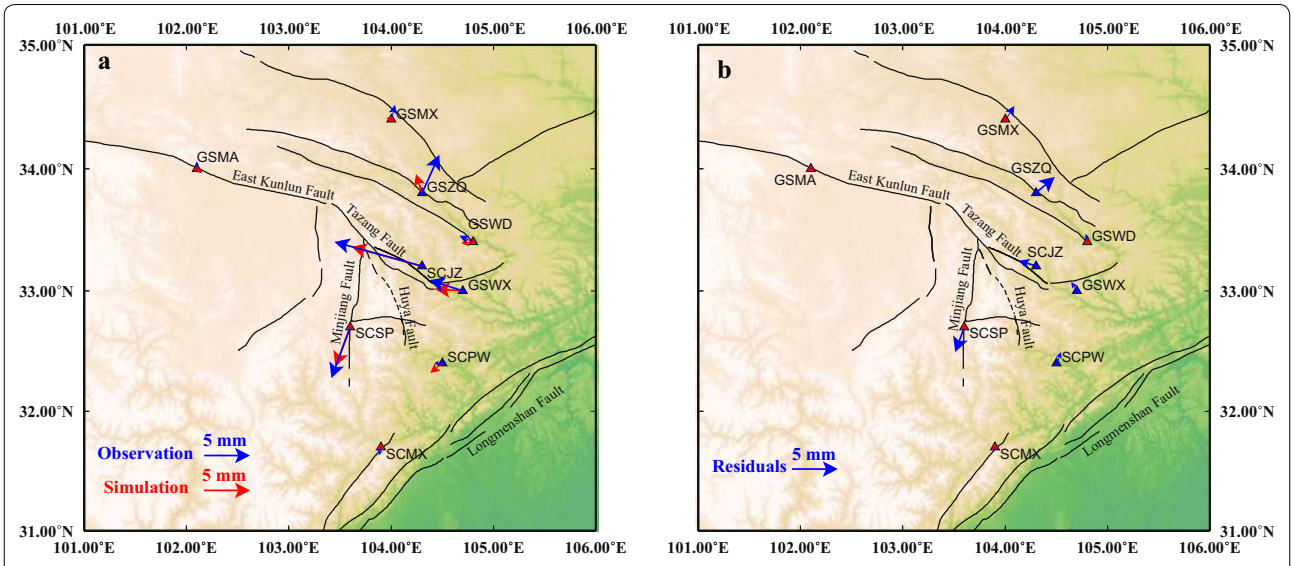

Fig. 5 **a** Observed and simulated coseismic deformation using GPS. **b** Horizontal residuals between observations and simulations

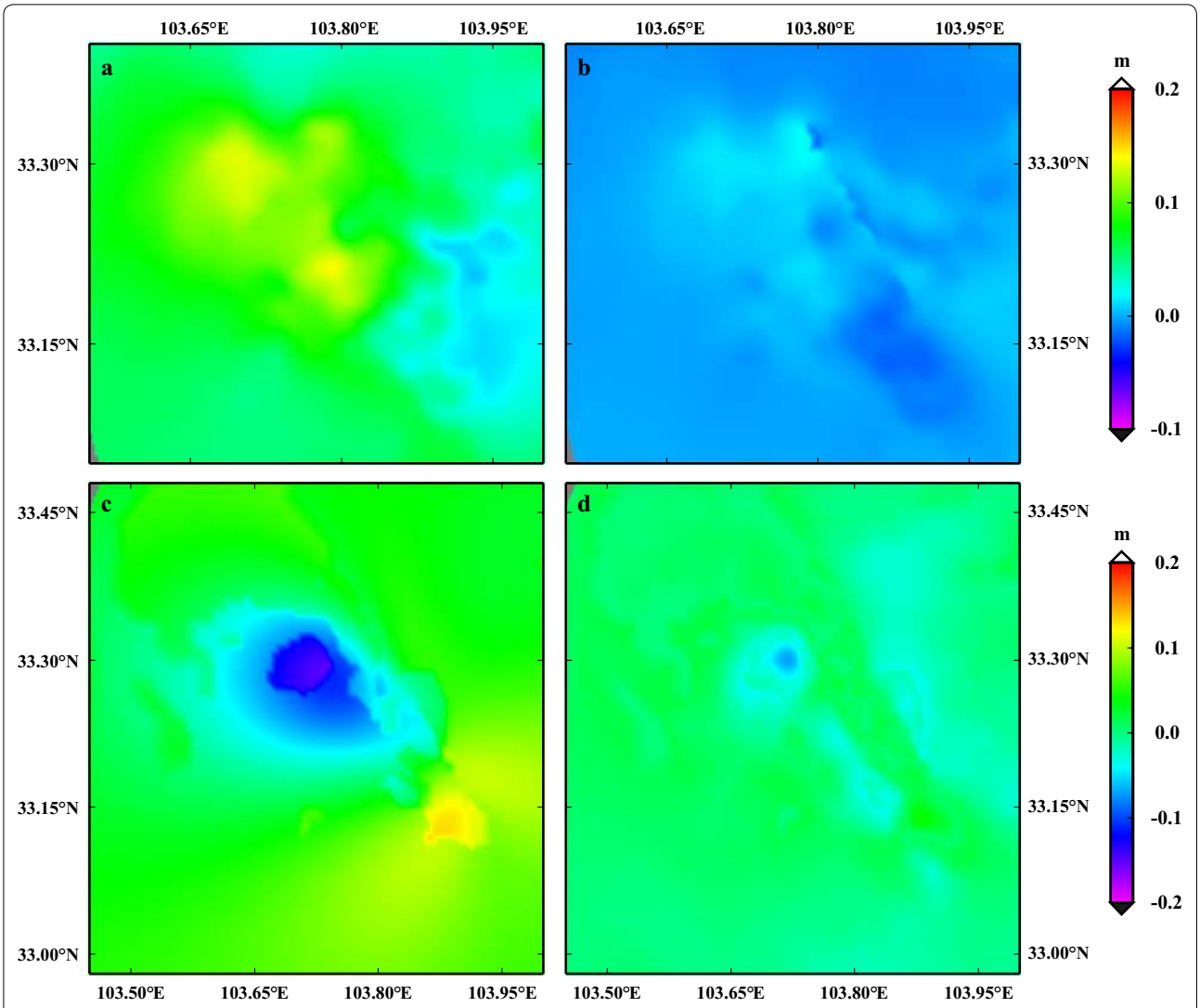

Fig. 6 Simulated coseismic deformation field and residuals for InSAR. **a**, **b** Present simulated coseismic deformation and residuals along the descending orbit. **c**, **d** Present simulated coseismic deformation and residuals along the ascending orbit

for those stations far from the epicenter were relatively greater because the observed coseismic displacements were small in these places. For example, all the stations presented a horizontal displacement from 1 to 2 mm except for GSZQ whose horizontal displacement was 3.5 mm. The simulated coseismic deformation and residual obtained for InSAR data showed that there was good consistency between simulated deformation and observed LOS displacement fields (Fig. 6). The residuals for InSAR were approximately −6 to 5 mm in the seismic region. The overall residual was approximately 2.5 mm, indicating that the coseismic slip distributions we obtained were reasonable.

Coseismic Coulomb stress analysis

According to the seismic stress trigger theory, the occurrence of one earthquake event will always lead to a stress redistribution at the epicenter and in its surrounding. The stress change field is not only highly correlated with the distribution of aftershocks, but also affects the seismic risk of the surrounding faults (Alin et al. 2008). Based on the Coulomb failure criterion, Coulomb stress changes are defined as follows:

$$\Delta\sigma_{\mathrm{f}} = \Delta\tau + \mu'\Delta\sigma_{\mathrm{n}} \tag{1}$$

where $\Delta\tau$ is the change in shear stress on the fault plane (the direction of the fault slipping is positive); $\Delta\sigma_{\mathrm{n}}$ is the change in normal stress (the tension direction of the fault

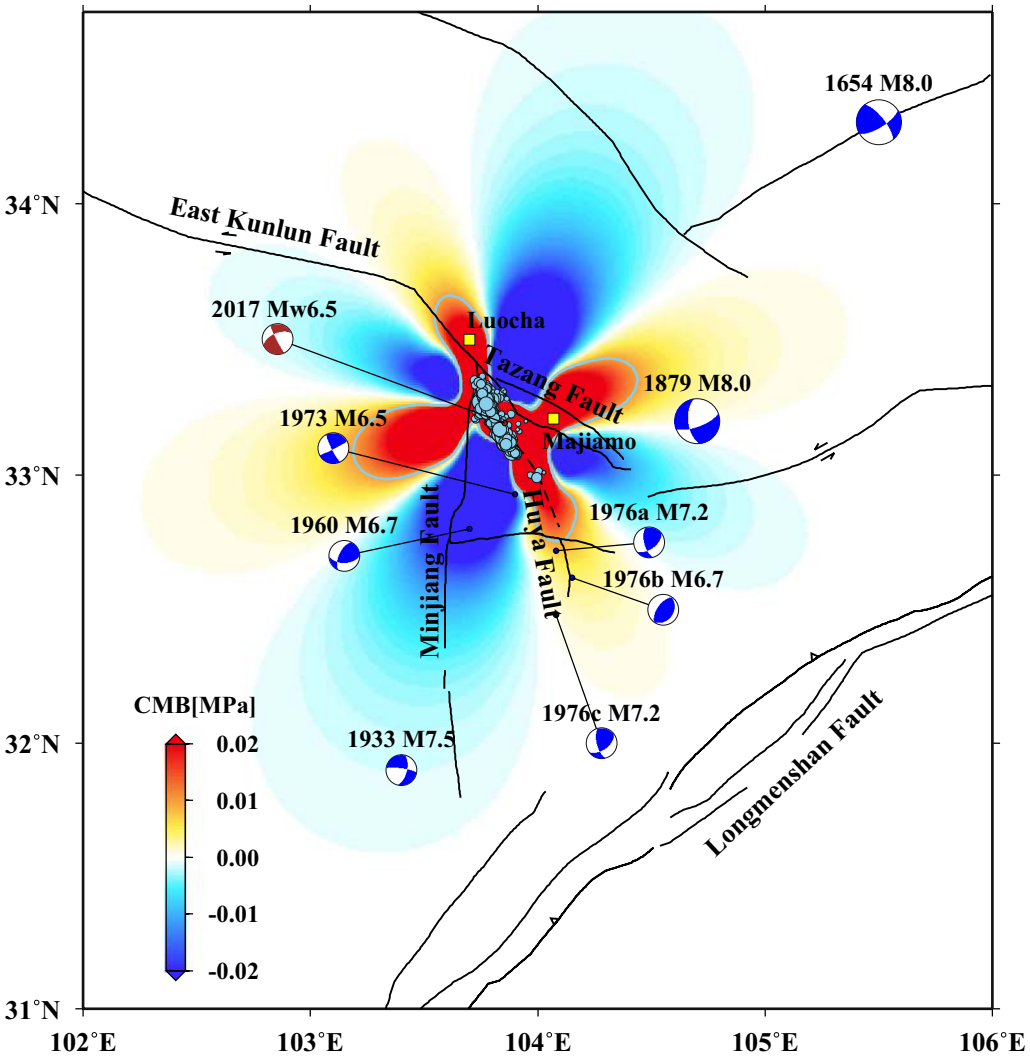

Fig. 7 Coseismic Coulomb stress changes of the Jiuzhaigou earthquake

is positive); and μ' is the effective friction coefficient; the Coulomb stress changes $\Delta\sigma_f$ will promote fault rupture if it is positive and delay fault rupture if it is negative. We used the PSCMP/PSGRN software package to calculate the coseismic Coulomb stress changes resulting from the Jiuzhaigou earthquake (Wang et al. 2006). The software is based on the layered viscoelastic half-space earth model, which can effectively simulate coseismic and postseismic deformation as well as stress changes. The depth of the Jiuzhaigou earthquake inferred from InSAR and GPS was 11 km. The effective friction coefficient used in the calculation is the common value 0.4 (King et al. 1994). The focal mechanism solutions of a large number of aftershocks are not clear, and the Coulomb stress changes of the optimal rupture plane can effectively explain the pattern of aftershock distributions (Shan et al. 2017a). Hence, we chose the optimal rupture plane as the received fault (Shan et al. 2011). The results showed that the coseismic Coulomb stress distribution resulting from the Jiuzhaigou earthquake was in good agreement with the aftershock distribution, and most of the aftershocks occurred in the region where the Coulomb stress increased (Fig. 7).

Calculation of the Coulomb stress changes on the optimal rupture plane is mainly used to determine the areas where the aftershocks might occur, but it cannot constrain the stress distribution of the other fault planes. Hence, for a specific fault, we need to apply the corresponding fault parameters to determine the Coulomb stress changes on the fault plane. The parameters of some

Table 3 Focal mechanism solutions of the Jiuzhaigou earthquake from different researchers

References	Strike	Dip (°)	Rake (°)	Depth (km)	Max. slip (m)	Magnitude (Mw)
Ji et al. (2017)	NW-NNW	70	/	9	0.77	6.46
Shan et al. (2017b)	153°	50	− 9	8	1	6.5
Zhang et al. (2017)	153°	84	− 19.5	11	1	6.5
Yi et al. (2017)	152°	70	/	5	/	6.4
This study	155°	81	− 11	11	0.85	6.49

received faults are from Xu et al. (2014) and Wan et al. (2009). The coseismic effect of the Jiuzhaigou earthquake caused significant stress increases greater than 0.01 MPa in the Luocha and Majiamo segments of the Tazang Fault, the Minjiang Fault, and the northern segment of the Huya Fault, while stress decreases in the middle and southern sections of the Minjiang Fault and the Tazang segment of the Tazang Fault. It is noted that four strong earthquakes with a magnitude $M > 6.5$ occurred in the Huya Fault from 1973 to 1976. Although the stress in most regions of the Huya Fault increased significantly after the Jiuzhaigou earthquake, the seismic risk in the ruptured area is considered low for the future. Zhang et al. (2012) argued that the Tazang Fault has the potential risk of a strong earthquake because the Luocha segment has experienced a Mw 7.3 earthquake during ancient times. The latest historical earthquake occurred on the Majiamo section of the Tazang Fault over 500 years ago (Fu et al. 2017). The seismic risk in this area is increasing because of the stress increase resulting from the Jiuzhaigou earthquake. Although the seismicity of the northern Minjiang Fault is weak, it is able to accumulate the strain energy necessary for a M7.0–7.5 earthquake (Zhou et al. 2000). The M6.8 Zhangla earthquake in 1960 is the latest earthquake to have occurred on the northern Minjiang Fault; no strong earthquakes have occurred in this area recently, which indicates that the seismic risk in the region is relatively high in the future.

Discussion

Precise determination of the position of the seismogenic fault of the Jiuzhaigou Mw 6.5 earthquake and its features can serve as an important clue for the understanding of tectonic characteristics and seismic activities of the region. Regarding the position of the epicenter determined by seismology, there are two types of opinions. One is that the earthquake is the result of extension of the Huya Fault in a NW direction, whereas the other suggests the activity is from the Tazang Fault. Because the epicenter position determined by seismology is not accurate (Zheng and Xie 2017), it is very important to determine the precise position of the epicenter using geodetic observations.

The coseismic deformation field obtained using InSAR data demonstrates an asymmetric distribution concentrated on the west side and with its major axis of deformation in a NW direction; it shows that the seismogenic fault is dipping to the west and has a trending direction to the NW (Fig. 1). The coseismic slip model shows that the fault is a SE-trending fault with a strike of 155°, a rake of − 11°, and a dip of 81° (Fig. 4). This shows that the earthquake was mainly triggered by a left-lateral strike-slip fault. The slip distribution model obtained from the geodetic observations of GPS and InSAR demonstrates that the Jiuzhaigou earthquake did not lead to surface rupture (Fig. 4). Field investigations also did not identify any obvious surface fractures (Xu et al. 2017). These results indicate that the seismogenic fault is a blind fault. Our result is consistent with that of Yi et al. (2017) and Zhang et al. (2017), but it differs from that of Ji et al. (2017) in terms of strike direction and that of Shan et al. (2017b) in terms of dip angle (Table 3). Yi et al. (2017) used the waveforms of the main shock and aftershocks to invert the focal mechanism. Zhang et al. (2017) applied the waveforms and InSAR to invert the focal mechanism. We believe the results from Yi et al. (2017) and Zhang et al. (2017) are more accurate.

The fault deformation characteristics obtained from geodetic inversion (coseismic) and GPS observations between 2013 and 2015 (interseismic) are different (Table 1). The discrepancies can largely be attributed to the sparseness of the GPS stations and their long distance from the fault. Meanwhile, the postseismic deformation resulting from the Wenchuan earthquake has also affected the results. Zhao (2017) demonstrated that the postseismic deformation in the Jiuzhaigou region caused by the Wenchuan earthquake was approximately 0.2 mm/a by the end of 2016. This result indicates that the effects of postseismic deformation resulting from the Wenchuan earthquake are negligible.

Hu et al. (2017) concluded that the western section of the Tazang Fault was dominated by horizontal shear motion and that the strike-slip component of the southeastern section gradually diminished. The Huya Fault is a left-lateral strike-slip fault with a thrust component and is roughly divided into northern and southern segments

by Xiaohe. The northern segment is dominated by strike-slip movement with a dipping direction to the NE and a dip angle of 80° (Ren et al. 2013). The southern segment inclines to the SW and is mainly controlled by inverse motion (Jones et al. 1984). Although the epicenter of the Jiuzhaigou earthquake is near the southeastern section of the Tazang Fault, the focal mechanism solution obtained in this study shows an obvious discrepancy from the geological characteristics of the southeastern section of the Tazang Fault. In contrast, the geometric features and focal mechanism solution of the seismogenic fault are very consistent with those of the northern section of the Huya Fault. The historical earthquake catalog of the Huya Fault shows three moderately strong earthquakes occurred in the southern section of the fault during 1976 and completely ruptured to the surface. However, seismic activities at the northern section of the Huya Fault have noticeably diminished following the Songpan–Huanglong M6.5 earthquake in 1973. Furthermore, the focal mechanism of the Jiuzhaigou earthquake is similar to that of the Songpan–Huanglong M6.5 earthquake of 1973 which, along with three other moderately strong earthquakes that occurred in Songpan during 1976, formed an earthquake belt with a NW-trending direction. Therefore, we believe the Jiuzhaigou earthquake could be the result of extensional activity along the northern section of the Huya Fault toward the NW. This result is consistent with Xu et al. (2017) and Yi et al. (2017), both of them suggest the Huya Fault belongs to one of the tail structures or branches at the easternmost end of the eastern Kunlun fault zone. Yi et al. (2017) defined the Shuzheng Fault as the seismogenic fault, which may be connected to the Huya Fault to the southeast. However, because the Shuzheng Fault has not been reported previously, we suggest the seismogenic fault of the Jiuzhaigou earthquake is the Shuzheng segment of the northern Huya Fault.

Based on the results of coseismic Coulomb stress changes, the Coulomb stress presented a clear incensement in four areas resulting from the Jiuzhaigou earthquake. The aftershocks were mainly concentrated at the NW and SE ends of the seismogenic fault. They trend in a N-NW direction, corresponding to the extension of the northern section of the Huya Fault. This demonstrates that the aftershocks were the result of a continuous energy release from the Huya Fault. This further shows that the Jiuzhaigou earthquake was the result of NW extension and fracture of the northern section of the Huya Fault. It should also be noted that no aftershocks were recorded in the stress-reinforced regions at the NW and SE edges of the seismogenic fault. Considering that the epicenter and its vicinity have similar structural stress fields, the absence of aftershocks is an indication that these regions are still in a locked state and the stress has not yet been released. The occurrence risk of a high-magnitude earthquake cannot be ignored in this region in the future. Conversely, the GPS deformation field from 2013 to 2015 indicated that although the slip rate of the northern section of the Huya Fault was faster than that of the southern section (Table 1), the slip model of the Jiuzhaigou earthquake presented a single point source model and did not result in surface rupture. This also indicates that it is likely that the stress has not yet been completely released and attention should be paid to the northern section of the Huya Fault regarding earthquake risk in the future.

The static Coulomb stress changes show that the stress increased beyond the earthquake trigger threshold of 0.01 MPa in the Luocha and Majiamo segments of the Tazang Fault, the northern Minjiang Fault, and the southern Huya Fault. Because the seismic activity of the southern Huya Fault is relatively weak and several strong earthquakes have occurred recently, the seismic risk of the southern Huya Fault is relatively low. However, the seismic risk for the Luocha and Majiamo segments of the Tazang Fault and the northern Minjiang Fault is increasing because strong earthquakes have not occurred in these areas in quite some time.

A series of strong earthquakes have occurred on the secondary active faults on the eastern and southeastern Tibetan Plateau including the Jiuzhaigou (Mw 6.5), Ludian (Mw 6.2), Jinggu (Mw 6.2), and Kangding (Mw 6.0) earthquakes since the great Mw 7.9 Wenchuan earthquake. The Bayan Har block is among the most frequently seismically active secondary blocks affected by strong earthquakes since the 1997 Manyi Mw 7.6 earthquake. Generally, frequent strong earthquakes in this region are mainly dominated by extrusion movement from the Tibetan Plateau. On the other hand, Coulomb stress changes induced from a strong earthquake can not only dissipate, but also move up and down fault segments, concentrating and promoting subsequent tremors (Toda 2008). It is necessary to assess the seismic hazard by analyzing the Coulomb stress changes caused by strong earthquakes on different fault planes, in cooperation with geodetic observations and seismic activities.

Conclusion

1. We obtained the coseismic deformation field of the Jiuzhaigou Mw 6.5 earthquake that occurred on August 8, 2017 using GPS and InSAR data. Kinematic characteristics have tentatively demonstrated a clear left-lateral slip characteristic of the earthquake. The coseismic slip model derived from a homogeneous elastic half-space inversion also shows that the earthquake was dominated by left-lateral slip. The earthquake rupture did not reach the ground sur-

face, consistent with emergency field investigations. The seismogenic fault is 40 km in length, 30 km in width, and has a strike of 155° with a dip angle of 81° and a rake angle of ~11°. The maximal fault slip is at 33.25°N, 103.82°E and at a depth of ~11 km. The moment was 6.635×10^{18} Nm, corresponding to a magnitude of Mw 6.49. This is consistent with the focal mechanism solutions provided by the USGS, GCMT, and other researchers.

2. Based on the coseismic slip model obtained from GPS and InSAR data, the coseismic static Coulomb stress, and the precise positions of aftershocks, the kinematic characteristics of the seismogenic fault do not match those of the southeastern section of the Tazang Fault but agree well with those of the northern section of the Huya Fault. These results indicate that the earthquake did not occur at the southeastern end of the Tazang Fault but instead occurred in the northern section of the Huya Fault. We define the seismogenic fault of the Jiuzhaigou earthquake as the Shuzheng segment of the northern Huya Fault, which is currently a blind fault.
3. Coseismic Coulomb stress resulting from the Jiuzhaigou earthquake increased at the NW and SE edges of the Shuzheng segment of the northern Huya Fault. The small number of aftershocks is an indication that the seismic risk in these regions cannot be ignored in the future.

Abbreviations

BGBAS: Beidou Ground Based Augmentation System; CMONOC: Crustal Movement Observation Network of China; ESA: European Space Agency; GCMT: Global Centroid Moment Tensor; GPS: Global Positioning System; InSAR: Interferometric Synthetic Aperture Radar; IW: interferometric wide; ISCE: InSAR Scientific Computing Environment software; JPL: Jet Propulsion Laboratory; LOS: line-of-sight; NASA: National Aeronautics and Space Administration; SRTM: Shuttle Radar Topography Mission; USGS: US Geological Survey.

Authors' contributions

ZN calculated coseismic Coulomb stress changes and drafted the manuscript. DW conducted the joint inversion of GPS and InSAR data to obtain the coseismic slip of finite fault model and helped to draft the manuscript. ZJ analyzed the GPS data to obtain coseismic deformation caused by the earthquake. PY analyzed the InSAR data and participated in the design of the study. LL participated in the fieldwork to obtain GPS data and the discussion of the study. All authors read and approved the final manuscript.

Acknowledgements

We are grateful to the European Space Agency for providing free SAR data. The InSAR Scientific Computing Environment (ISCE) software jointly developed by the JPL and Stanford University was used for processing the InSAR data. The precision orbits released by the European Space Agency and the 30-m-resolution SRTM digital elevation model of NASA were also used for terrain elimination. Generic Mapping Tools (GMTs) provided by Wessel and Smith (1998) were used to develop the figures. We are thankful to B. Zhao, R. Zhang, Y. Li, and H. Shi for their kind assistance. We thank the anonymous reviewers and the editor for their helpful comments to improve our manuscript.

Ethics approval and consent to participate

Not applicable.

Competing interests

The authors declare that they have no competing interests.

Funding

This research was supported by funding from the National Natural Science Foundation of China (Grant Nos. 41504011, 41474097) and the Science for Earthquake Resilience of China Earthquake Administration (XH17023Y).

Publisher's Note

Received: 20 November 2017 Accepted: 27 March 2018
Published online: 10 April 2018

References

Alin ST, Freed AM, Calais E et al (2008) Coulomb stress evolution in Northeastern Caribbean over the past 250 years due to coseismic, postseismic and interseismic deformation. Geophys J Int. https://doi.org/10.1111/j.1365246X.2008.03634.x

Deng QD, Chen SP, Ma J, Du P (2014) Seismic activities and earthquake potential in the Tibetan Plateau. Chin J Geophys. https://doi.org/10.6038/cjg20140701 **(in Chinese with English abstract)**

Farr TG, Kobrick M (2000) Shuttle radar topography mission produces a wealth of data. Eos Trans Am Geophys Union 81:583–585

Fu GC, Zhang JL, Cai YY (2017) Late Quaternary tectonic activity on the Majiamo segment of the Tazang fault. Earthquake 37(3):51–60 **(in Chinese with English abstract)**

Goldstein RM, Werner CL (1998) Radar interferogram filtering for geophysical applications. Geophys Res Lett 25(21):4035–4038. https://doi.org/10.1029/1998GL900033

Hu CZ, Ren JW, Yang PX et al (2017) Discussion on the compression-shear activity of the Tazang fault in East Kunlun and uplift of plateau. Acta Geol Sin 91(7):1401–1415 **(in Chinese with English abstract)**

Ji LY, Liu CJ, Xu J et al (2017) InSAR observation and inversion of the seismogenic fault for the 2017 Jiuzhaigou Ms7.0 earthquake in China. Chin J Geophys. https://doi.org/10.6038/cjg20171032 **(in Chinese with English abstract)**

Jones LM, Han WB, Hauksson E et al (1984) Focal mechanisms and aftershock locations of the Songpan earthquakes of August 1976 in Sichuan, China. J Geophys Res Solid Earth. https://doi.org/10.1029/jb089ib09p07697

King GCP, Stein RS, Lin J (1994) Static stress changes and the triggering of earthquakes. Bull Seismol Soc Am 84:935–953

Kirby E, Harkins N, Wang EQ et al (2007) Slip rate gradients along the eastern Kunlun fault. Tectonics. https://doi.org/10.1029/2006TC002033

Liu M, Mooney W, Li S (2006) Crustal structure of the northeastern margin of the Tibetan plateau from the Songpan-Ganzi terrane to the Ordos basin. Tectonophysics. https://doi.org/10.1016/j.tecto.2006.01.025

Lohman RB, Sinmons M (2005) Some thoughts on the use of InSAR data to constrain model of surface deformation: noise structure and data downsampling. Geochem Geophys Geosyst. https://doi.org/10.1029/2004GC000841

Okada Y (1985) Surface deformation due to shear and tensile faults in a half-space. Bull Seismol Soc Am 75(4):1135–1154

Parsons B et al (2006) The 1994 Sefidabeh (eastern Iran) earthquakes revisited: new evidence from satellite radar interferometry and carbonate dating about the growth of an active fold above a blind thrust fault. Geophys J Int. https://doi.org/10.1111/j.1365-246X.2005.02655.x

Ren JJ, Xu XW, Yeats RS, Zhang SM (2013) Millennial slip rates of the Tazang fault, the eastern termination of Kunlun fault: implications for strain partitioning in eastern Tibet. Tectonophysics. https://doi.org/10.1016/j.tecto.2013.06.026

Shan B, Xiong X, Zheng Y et al (2011) The co-seismic Coulomb stress change and expected seismicity rate caused by 14 April 2010 Ms = 7.1 Yushu, China, earthquake. Tectonophysics. https://doi.org/10.1016/j.tecto.2011.08.003

Shan B, Xiong X, Jin BK et al (2012) Earthquake stress interaction in the northeastern Songpan-Ganzi block and its implication for earthquake hazard. Chin J Geophys. https://doi.org/10.6038/j.issn.0001-5733.2012.07.018 **(in Chinese with English abstract)**

Shan B, Zheng Y, Liu CL, Xie ZJ, Kong J (2017a) Coseismic Coulomb failure stress changes caused by the 2017 M7.0 Jiuzhaigou earthquake, and its relationship with the 2008 Wenchuan earthquake. Sci China Earth Sci. https://doi.org/10.1007/s11430-017-9125-2 **(in Chinese with English abstract)**

Shan XJ, Qu CY, Gong WY et al (2017b) Coseismic deformation field of the Jiuzhaigou Ms7.0 earthquake from Sentinel-1A InSAR data and fault slip inversion. Chin J Geophys. https://doi.org/10.6038/cjg20171201

Stein RS (2003) Earthquake conversations. Sci Am. https://doi.org/10.1038/scientificamerican0103-72

Tang RC, Lu LK (1981) On the seismogeological characteristics of 1976 Songpan-Pingwu earthquakes. Seismol Geol 3(2):41–47 **(in Chinese with English abstract)**

Toda S (2008) Coulomb stresses imparted by the 25 March 2007 Mw = 6.6 Noto-Hanto, Japan, earthquake explain its 'butterfly' distribution of aftershocks and suggest a heightened seismic hazard. Earth Planets Space. https://doi.org/10.1186/bf03352866

Wan YG, Shen ZK, Sheng SZ et al (2009) The influence of 2008 Wenchuan earthquake on surrounding faults. Acta Geophys Sin 31(2):128–139 **(in Chinese with English abstract)**

Wang RJ, Lorenzo-Martín F, Roth F (2006) PSGRN/PSCMP—a new code for calculating co- and post-seismic deformation, geoid and gravity changes based on the viscoelastic-gravitational dislocation theory. Comput Geosci. https://doi.org/10.1016/j.cageo.2005.08.006

Wang C, Han W, Wu J et al (2007) Crustal structure beneath the eastern margin of the Tibetan Plateau and its tectonic implications. J Geophys Res Solid Earth. https://doi.org/10.1029/2005jb003873

Wang Y, Wang E, Shen Z et al (2008) GPS-constrained inversion of present-day slip rates along major faults of the Sichuan-Yunnan region, China. Chin Sci Earth Sci 51(09):1267–1283

Wang CS, Ding XL, Li QQ, Jiang M (2014) Equation-based InSAR data quadtree down sampling for earthquake slip distribution inversion. IEEE Geosci Remote Sens Lett. https://doi.org/10.1109/LGRS.2014.2318775

Wang Y, Gan W, Chen W et al (2018) Coseismic displacements of the 2017 Jiuzhaigou M7.0 earthquake observed by GNSS: preliminary results. Chin J Geophys. https://doi.org/10.6038/cjg2018l0611 **(in Chinese with English abstract)**

Wells D, Coppersmith K (1994) New empirical relationships among magnitude, rupture length, rupture width, rupture area, and surface displacement. Bull Seismol Soc Am 84(4):974–1002

Wessel P, Smith WH (1998) New, improved version of generic mapping tools released. Eos Trans Am Geophys Union 79(47):579–578

Xiong W, Tan K, Liu G et al (2015) Coseismic and postseismic Coulomb stress changes on surrounding major faults caused by the 2015 Nepal Mw7.9 earthquake. Chin J Geophys. https://doi.org/10.6038/cjg20151135 **(in Chinese with English abstract)**

Xu J, Shao ZG, Ma HS et al (2014) Impact of the 2008 Wenchuan 8.0 and the 2013 Lushan 7.0 earthquakes along the Longmenshan fault zone on surrounding faults. Earthquake 34(04):40–49 **(in Chinese with English abstract)**

Xu XW, Chen GH, Wang QX et al (2017) Discussion on seismogenic structure of Jiuzhaigou earthquake and its implication for current strain state in the southeastern Qinghai-Tibet Plateau. Chin J Geophys. https://doi.org/10.6038/cjg20171028 **(in Chinese with English abstract)**

Yi GX, Long F, Liang MJ et al (2017) Focal mechanism solutions and seismogenic structure of the 8 August 2017 M7.0 Jiuzhaigou earthquake and its aftershocks, northern Sichuan. Chin J Geophys. https://doi.org/10.6038/cjg20171033 **(in Chinese with English abstract)**

Zhang JL, Ren JW, Fu JD et al (2012) The earthquake rupture features and tectonic significance of the Tazang fault in eastern part of the east Kunlun fault zones. Earthquake 32(1):1–16 **(in Chinese with English abstract)**

Zhang X, Feng WP, Xu LS et al (2017) The source-process inversion and the intensity estimation of the 2017 Ms7.0 Jiuzhaigou earthquake. Chin J Geophys. https://doi.org/10.6038/cjg20171035 **(in Chinese with English abstract)**

Zhao B (2017) Exploring the lithospheric rheological structure of the eastern and southern Tibetan Plateau by postseismic GPS data. Doctoral Thesis, Wuhan University, China

Zhou RJ, Pu XH, He YL et al (2000) Recent activity of Mingjiang fault zone, uplift of Minshan block and their relationship with seismicity of SiChuan. Seismology and Geology 22(3): 285-294 (**in Chinese with English abstract**)

Zheng Y, Xie ZJ (2017) Present status and prospect of earthquake focal depth locating. J Seismol Res 40(2):167–175

Zhou RJ, Li Y et al (2007) Active tectonics of the Longmen Shan region on the eastern margin of the Tibetan Plateau. Acta Geol Sin. https://doi.org/10.1111/j.1755-6724.2007.tb00983.x